Energy & Environmental Science

Cite this: *Energy Environ. Sci.*, 2012, **5**, 7963

www.rsc.org/ees

PAPER

Low effective mass leading to high thermoelectric performance

Yanzhong Pei, Aaron D. LaLonde, Heng Wang and G. Jeffrey Snyder*

Received 3rd March 2012, Accepted 24th April 2012
DOI: 10.1039/c2ee21536e

High Seebeck coefficient by creating large density-of-states effective mass through either electronic structure modification or manipulating nanostructures is commonly considered as a route to advanced thermoelectrics. However, large density-of-state due to flat bands leads to large transport effective mass, which results in a simultaneous decrease of mobility. In fact, the net effect of such a high effective mass is a lower thermoelectric figure of merit, zT, when the carriers are predominantly scattered by phonons according to the deformation potential theory of Bardeen–Shockley. We demonstrate that the beneficial effect of light effective mass contributes to high zT in n-type thermoelectric PbTe, where doping and temperature can be used to tune the effective mass. This clear demonstration of the deformation potential theory to thermoelectrics shows that the guiding principle for band structure engineering should be low effective mass along the transport direction.

Increasing the thermoelectric figure of merit (zT) is the most challenging task to enable the widespread use of this method to directly convert heat into electricity. The transport properties including resistivity (ρ), Seebeck coefficient (S), electronic (κ_E) and lattice (κ_L) components of thermal conductivity ($\kappa = \kappa_E + \kappa_L$) determine the figure of merit, $zT = S^2T/\rho\kappa$, where T is the absolute temperature.

Creating phonon scattering centers such as nanostructures[1–6] to lower κ_L has been proven effective for achieving $zT > 1$ in many instances. However, κ_L in such materials already approaches its amorphous limit,[3,4] suggesting strategies targeting increases in zT by improvements of the thermoelectric power factor (S^2/ρ).

The decoupling of S, ρ and κ_E in an effort to achieve high zT has been a longstanding challenge as they are strongly coupled with each other through the carrier concentration, scattering and band structure.[7–9] However, it is well known that the optimal electronic performance of a thermoelectric semiconductor depends primarily on the weighted mobility,[9–12] $\mu(m^*/m_e)^{3/2}$, which includes both the density-of-states effective mass (m^*, m_e is the free electron mass) and the nondegenerate mobility (μ) of carriers.

More generally, each degenerate carrier pocket makes a contribution to m^* *via* $m^* = N_v^{2/3}m_b^*$,[9–13] where N_v and m_b^* are the number of degenerate carrier pockets and the average band mass (density-of-states effective mass for each pocket), respectively. Without explicitly reducing μ, converging many valence (or conduction) bands to achieve high N_v and therefore a high m^* has been proposed as an effective approach to high performance in both bulk[14,15] and low dimensional[16] thermoelectrics.

In an attempt to increase the power factor, without modifying N_v, many efforts have been recently devoted to increasing the Seebeck coefficient (*i.e.* increasing m^* through high m_b^*) either by designing[17,18] the density-of-states or manipulating nanostructures.[19,20] This concept has recently been considered as a criterion[11,12] for obtaining good thermoelectrics. However, these methods may reduce the mobility significantly.[18]

Materials Science, California Institute of Technology, Pasadena, CA 91125, USA. E-mail: jsnyder@caltech.edu

Broader context

Thermoelectric generators that directly convert heat into electricity are now actively considered for a variety of waste heat recovery systems (such as the conversion of automobile exhaust heat into electricity) to combat the global energy dilemma. Driven by a large Seebeck coefficient at a given carrier concentration, materials having a high effective mass are generally pursued to achieve high thermoelectric performance. However, this is effective only when the large effective mass originates from highly degenerated electronic bands. Under a scattering mechanism of carriers for most of the good thermoelectrics, increasing the effective mass for each band without increasing the band degeneracy reduces the carrier mobility significantly enough to overwhelm the resulting increase in Seebeck coefficient, therefore leading to a net decrease in the thermoelectric power factor. Contrary to the general belief, low effective mass for each band is demonstrated to be beneficial for high performance thermoelectrics.

In fact, an increase of m^* resulting from increasing m_b^* (*i.e.* by flattening the band) leads to a significant decrease in mobility according to the deformation potential theory of Bardeen–Shockley.[21] This is because $\mu \propto m_b^{*-3/2} m_I^{*-1}$ (m_I^*, inertial mass of the carriers along the conducting direction)[21–23] when the carriers are predominantly scattered by non-polar phonons (either acoustic or optical), as has been found in most of the known and good thermoelectrics. As a result, the optimal $zT \propto \mu m^{*3/2} \propto N_v m_I^{*-1}$ becomes inversely proportional to m_I^*.[9,10,24,25] Since cubic thermoelectric materials such as PbTe, SiGe and skutterudites have an isotropic m_I^* that is directly related to m_b^*,[26] it is clear that increasing m_b^* actually decreases the optimal power factor in spite of the resulting large Seebeck coefficient.

In this paper we demonstrate that a lower effective mass (either by doping or by adjusting the temperature) leads to a high power factor and thus excellent thermoelectric performance in n-PbTe. When compared with La-doped PbTe, a ~20% lower effective mass in I-doped PbTe results in a ~20% higher power factor and higher zT. This work shows a contrasting example to the commonly utilized strategy for large Seebeck coefficients resulting from heavy band mass for high performance thermoelectrics.[11,17,19,20]

La- and I-doped PbTe ($La_xPb_{1-x}Te$ and $PbTe_{1-x}I_x$ with $0 < x < 0.01$) were synthesized by the same melting, quenching, annealing and hot pressing methods. The synthesis procedure and details of the measurement of transport properties can be found elsewhere.[27,28] It should be noted that the transport properties were measured on hot pressed pellets with a theoretical density $d \geq 98\%$. The thermal conductivity was calculated *via* $\kappa = dC_pD$, where D is the measured thermal diffusivity using the laser flash method (Netzsch LFA 457). Heat capacity (C_p) is estimated by C_p (k_B per atom) = 3.07 + 4.7 × 10^{-4} × (T/K − 300), which is obtained by fitting the experimental data reported by Blachnik[29] within an uncertainty of 2% for all the lead chalcogenides at $T > 300$ K. It should be emphasized that this simple equation agrees well with the theoretical prediction[30] taking the lattice vibration (Debye temperature[24] of 130 K), dilation (bulk modulus[31] of 40 GPa, the linear coefficient[24] of thermal expansion of 20 × 10^{-6} K^{-1}) and charge carrier contributions into account. Furthermore, this equation enables a reasonable estimate of composition dependent C_p for lead chalcogenide materials that are typically used,[6,14,27,29,32–35] within an uncertainty of 5%. Fig. 1 shows the C_p (in J g^{-1} K^{-1}) for PbTe that is used in this work (solid curve), comparing with literature results for PbTe[29,35] and PbTe with dilute impurities.[1,36–38] At 700 K or above this equation gives $C_p \approx 10\%$ higher than the Dulong–Petit value as shown in Fig. 1. The measurement uncertainty for each transport property (S, σ and D) is about 5%.

In both La- and I-doped PbTe the donor states are very shallow[39] so that each dopant atom produces one electron[28] in the conduction band according to the rules of valence.[40] The Hall carrier concentration ($n_H = 1/eR_H$, e is the electron charge) is determined from the measured Hall coefficient (R_H), and the room temperature values of n_H are used to identify the samples. All the samples in this study show n-type conduction. La- and I-doped PbTe samples with two important Hall carrier concentrations of ~1.8 and ~3 × 10^{19} cm^{-3}, which respectively enable the highest average zT and peak zT in the temperature range of most interest for thermoelectric applications, were chosen for the discussion of temperature dependent transport properties. To avoid the detrimental effects due to minority carriers[15,41] (Fig. 2) and to validate the use of the single band conduction model as discussed below, we focus on the transport properties from 300 K to 600 K for comparing the electronic properties. For temperatures or carrier concentration, where the scattering is not dominated by acoustic (nonpolar) phonons or the transport properties are not sufficiently described by a single band model, the following analysis and conclusions are not applicable.

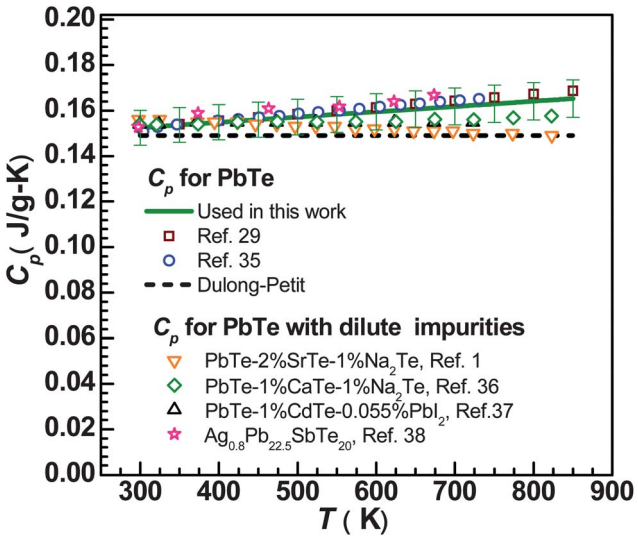

Fig. 1 Temperature dependent heat capacity (C_p) for PbTe and PbTe with dilute impurities. The solid curve (with a 5% error bar) represents the heat capacity used here: C_p (k_B per atom) = 3.07 + 4.7 × 10^{-4} × (T/K − 300).

The measured Seebeck coefficient, resistivity, thermal conductivity and zT are shown in Fig. 2 as a function of temperature. The monotonically increasing Seebeck coefficient and resistivity, as well as the slightly (<10%) increased Hall coefficient (which can be expected from a slight loss of degeneracy, not shown), with increasing temperature allow the assumption of single band conduction behavior at $T < \sim 600$ K to be made in this study. This assumption is consistent with band structure studies of PbTe.[24]

It has been well known that the bands located at the L point ($N_v = 4$) of the Brillouin zone for PbTe are nonparabolic[24,42–44] and can be well described by a single Kane band model (SKB).

Furthermore, the scattering of charge carriers in PbTe is known to be dominated by acoustic phonons[24,45] in the temperature and carrier concentration range having high thermoelectric performance, as is the case for most good thermoelectric materials. This is demonstrated in Fig. 3a which shows that the Hall mobility decreases sharply with temperature ($\mu \approx T^p$ where $p < -1.5$, ref. 24). Other scattering mechanisms such as by grain boundaries, polar-optical phonons, and ionized impurities predict $p \geq -1/2$ implying that these mechanisms do not dominate the transport properties. In fact, the Hall mobility predicted by SKB with the acoustic scattering theory[21,22] and temperature dependent m^* (Fig. 3b) agrees well with the experimental data (Fig. 3a), for both La- and I-doped PbTe.

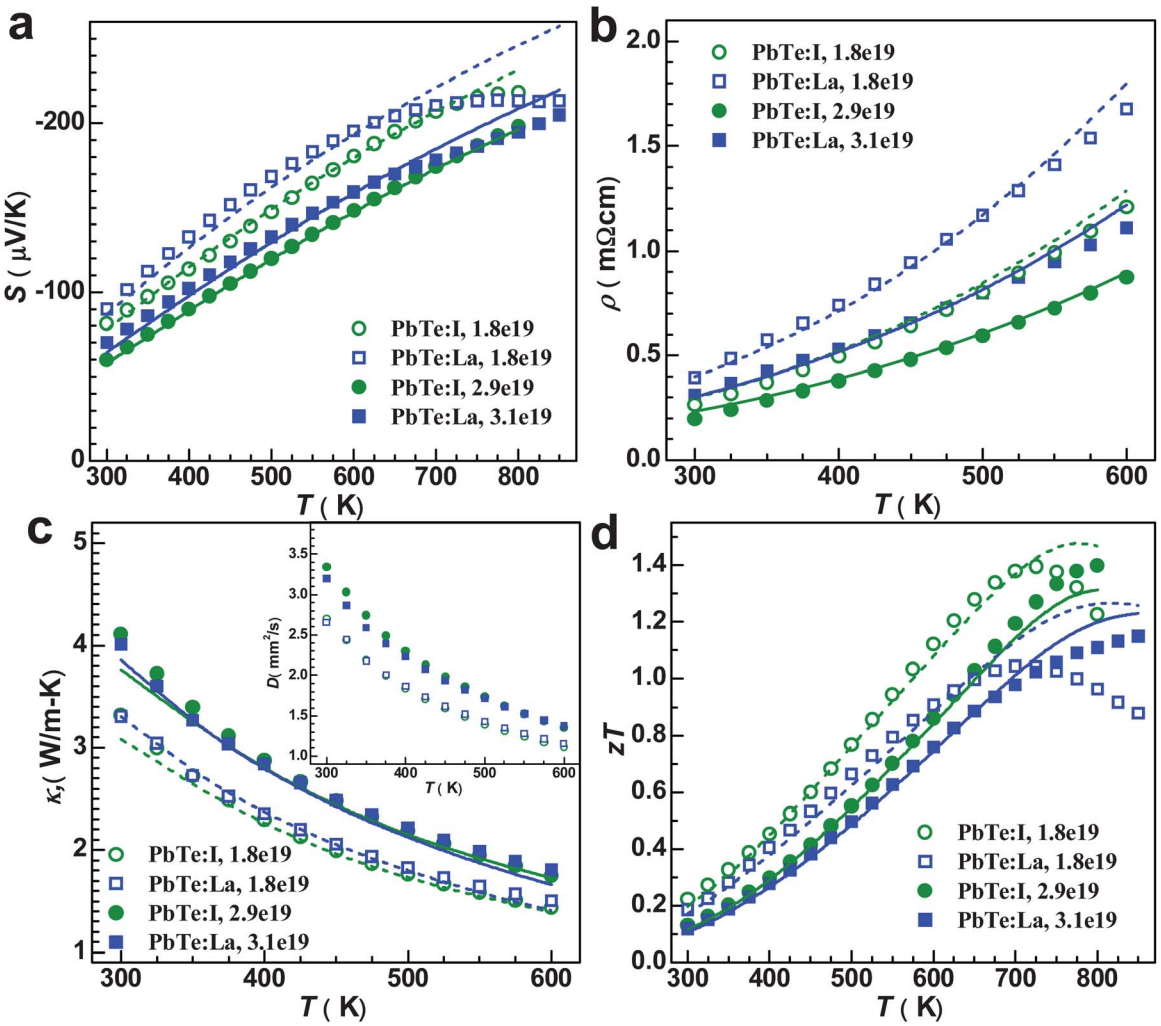

Fig. 2 Temperature dependent Seebeck coefficient (a), resistivity (b), thermal conductivity (c), thermal diffusivity (inset) and thermoelectric figure of merit (d) for two groups of La- and I-doped PbTe having room temperature Hall carrier concentration of ~1.8 and ~3 × 10^{19} cm^{-3}, respectively. The curves represent the predicted results from the single Kane band model with an effective mass of 0.25m_e for I-doping and 0.30m_e for La-doping, respectively. Comparing with La-doped PbTe that has nearly the same carrier concentration, higher figure of merit in I-doped sample is due to its lower effective mass over the whole temperature considered.

Such a Kane band model provides the expressions for the transport coefficients[24,42] as follows:Hall carrier density

$$n_H = \frac{1}{eR_H} = A^{-1}\frac{N_v(2m_b^* k_B T)^{3/2}}{3\pi^2\hbar^3}{}^0F_0^{3/2} \quad (1)$$

Hall factor

$$A = \frac{3K(K+2)}{(2K+1)^2}\frac{{}^0F_{-4}^{1/2}\cdot{}^0F_0^{3/2}}{({}^0F_{-2}^1)^2} \quad (2)$$

Hall mobility

$$\mu_H = A\frac{2\pi\hbar^4 eC_l}{m_I^*(2m_b^* k_B T)^{3/2}E_{def}^2}\frac{{}^3F_{-2}^1}{{}^0F_0^{3/2}} \quad (3)$$

Seebeck coefficient

$$S = \frac{k_B}{e}\left[\frac{{}^1F_{-2}^1}{{}^0F_{-2}^1} - \xi\right] \quad (4)$$

and Lorenz number

$$L = \left(\frac{k_B}{e}\right)^2\left[\frac{{}^2F_{-2}^1}{{}^0F_{-2}^1} - \left(\frac{{}^1F_{-2}^1}{{}^0F_{-2}^1}\right)^2\right] \quad (5)$$

where ${}^nF_k^m$ has a similar form as the Fermi integral:

$${}^nF_k^m = \int_0^\infty\left(-\frac{\partial f}{\partial\varepsilon}\right)\varepsilon^n(\varepsilon+\alpha\varepsilon^2)^m\left[(1+2\alpha\varepsilon)^2+2\right]^{k/2}d\varepsilon \quad (6)$$

In the above equations, k_B is the Boltzmann constant, $\hbar$ the reduced Planck constant, C_l the combined elastic moduli,[22] E_{def} the deformation potential coefficient[22] characterizing the strength of carriers scattered by acoustic phonons, ξ the reduced Fermi level, ε the reduced energy of the electron state, α (= k_BT/E_g) the reciprocal reduced band separation (E_g, at L point of the Brillouin zone in this study) and f the Fermi distribution. This model also considers an ellipsoidal Fermi surface by taking the ratio of the longitudinal ($m_\parallel^*$) to transverse ($m_\perp^*$)

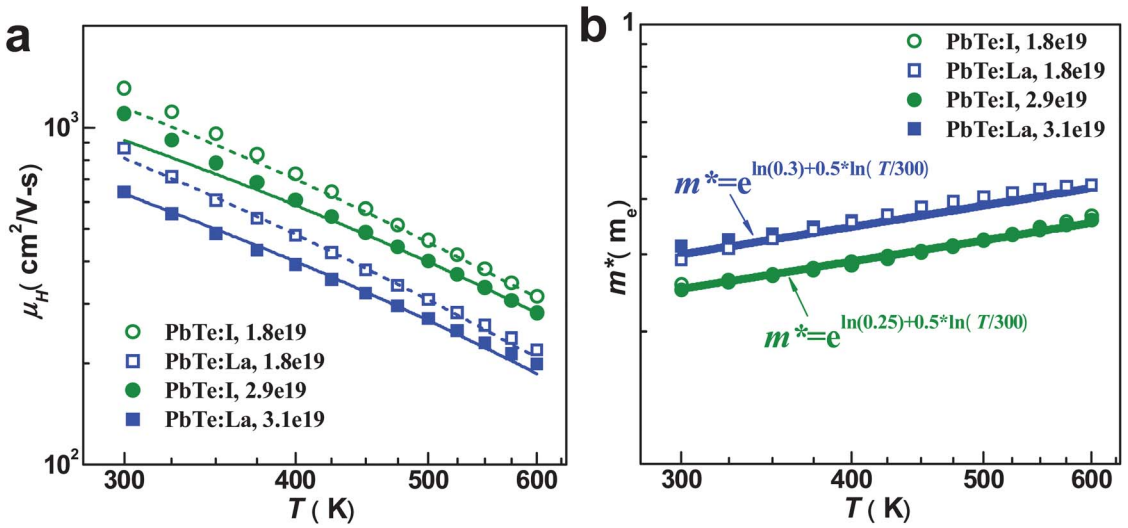

Fig. 3 Temperature dependent Hall mobility (a) and effective mass (b) for La- and I-doped PbTe. The experimental Hall mobility (symbols) can be well predicted (curves) by an acoustic scattering mechanism. La-doping leads to a ~20% higher effective mass over the entire temperature range. The increase in effective mass with increasing temperature is due to the Kane type band structure and is associated with the temperature dependent band gap.

effective mass components of the cigar-shaped carrier pocket into account *via* the term $K = m^*_{\parallel}/m^*_{\perp}$.

Utilizing the above SKB model, excellent prediction of the Hall carrier concentration dependent Seebeck coefficient and Hall mobility can be obtained for both La- and I-doped PbTe over a broad carrier concentration range as shown in Fig. 4. Literature data from different sources[28,46–52] show good consistency with the current work.

It is seen that the La-doped series shows slightly higher Seebeck coefficient values at both 300 K (Fig. 4a) and 600 K (Fig. 4b), which correspondingly means a higher density-of-states effective mass by 20% than that in the I-doped samples. Quantitatively, m^* is found to be $0.25 \pm 0.03m_e$ and $0.30 \pm 0.02m_e$ at 300 K, and $0.35 \pm 0.02m_e$ and $0.41 \pm 0.02m_e$ at 600 K, for I- and La-doped PbTe, respectively, where the standard deviations are obtained on approximately 10 different samples. Most importantly, only varying m^* by 20% enables an accurate prediction (curves in Fig. 4c and d) of the Hall mobility at both 300 and 600 K using the SKB model without any other adjustable parameters. Here, the values $K = 3.6$,[53] $C_l = 7.1 \times 10^{10}$ Pa,[45] $E_{def} = 22$ eV[28] and $\alpha = k_B T/(0.18\ \text{eV} + 0.0004\ \text{eV}/K \times T)$[24,54–56] are used for both I- and La-doped series. The excellent agreement between the experimental and predicted results confirms the validity of the model itself and additionally indicates that the higher m^* is indeed responsible for the observed higher S and lower μ_H.

The higher m^* in La-doped PbTe is presumably due to the conduction band flattening, related to an increase in band gap[46] according to the Kane dispersion $E(k)$:[42,57]

$$\frac{\hbar k^2}{2m^*} = E\left(1 + \frac{E}{E_g}\right) \quad (7)$$

In a Kane band system, the increase of m^* with increasing band gap has been theoretically predicted[24,58] and experimentally confirmed[33,44,53,59,60] in lead chalcogenides. Furthermore, the increase of m^* in PbTe and related materials can be induced by either temperature[24,53,59] or chemical substitution,[18] making available an additional tunable parameter for further investigation of m^* dependent thermoelectric properties.

With the knowledge of band separation at L point of the Brillouin zone, one can calculate the reduced Fermi level from the experimental Seebeck coefficient according to eqn (4). Consequently, m^* can be obtained from eqn (1) and (2). In this way, we calculate the temperature dependent m^* (Fig. 3b) for both La- and I-doped PbTe having room temperature Hall carrier concentrations of ~1.8 and ~3×10^{19} cm^{-3}. It is clearly seen that the 20% higher m^* in the La-doped series persists throughout the entire temperature range. Largely resulting from the lattice expansion,[24] the band gap increases with increasing temperature leading to an increase in m^* as theoretically predicted[24,58] and experimentally observed[33,44,53,59,60] in Kane band systems (eqn (7)). Therefore, the observed increase in m^* with increasing temperature by $d\ln m^*/d\ln T = 0.5$ (curves) can be well understood by the SKB model.[24,53,59]

With a combination of the predicted Hall carrier concentration dependent Seebeck and Hall mobility, the thermoelectric power factor (PF = $S^2 n_H e \mu_H$) is calculated and compared with the experimental data for the La- and I-doped series at 300 and 600 K in Fig. 5. It is clear that ~20% higher m^* leads to ~20% lower peak PF in La-doped series at both 300 K (34 *vs.* 28 μW cm^{-1} K^{-2}) and 600 K (25 *vs.* 21 μW cm^{-1} K^{-2}). Moreover, the temperature induced ~40% increase in m^* correspondingly results in a ~35% decrease in maximal PF for both La- (28 *vs.* 21 μW cm^{-1} K^{-2}) and I-doped (34 *vs.* 25 μW cm^{-1} K^{-2}) PbTe, as temperature rises from 300 to 600 K. An increase of m^* due to independent mechanisms leads to a reduction of the overall optimal thermoelectric power factor, despite the resulting increase of the Seebeck coefficient.

The physics behind why a higher m^* without increasing N_v has a detrimental effect on thermoelectric performance is similar for the SKB model as it is for a parabolic band model. Combining eqn (1), (3) and (4), one obtains:

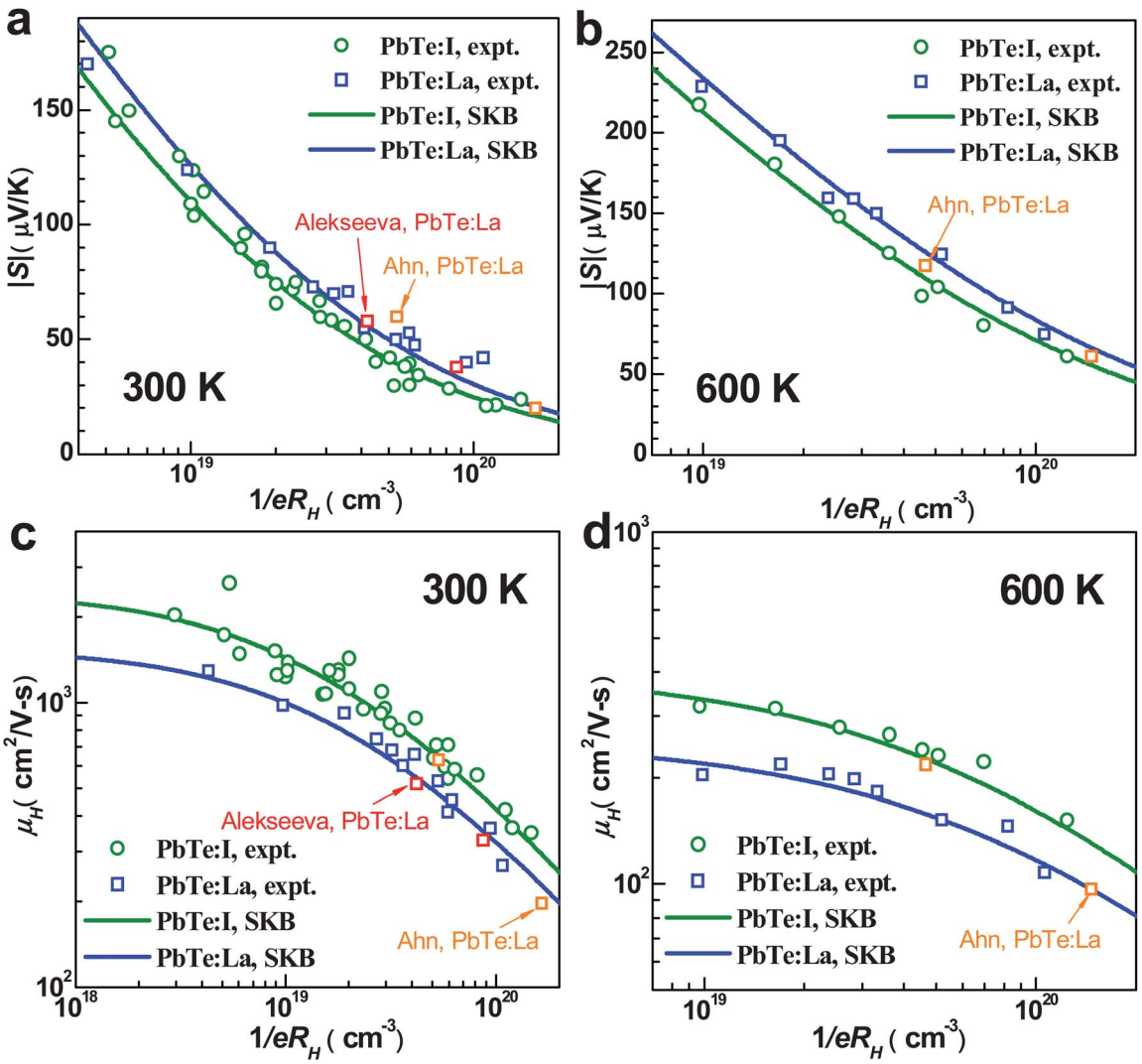

Fig. 4 Hall carrier concentration *versus* Seebeck coefficient (a and b) and Hall mobility (c and d) for I- and La-doped PbTe at 300 K (a and c) and 600 K (b and d), compared with the predicted results (curves) according to the single Kane band model. Providing a 20% higher effective mass in La-doped series, both the increase in Seebeck coefficient and decrease in Hall mobility can be well predicted by the SKB model.

$$\mathrm{PF} = \frac{2N_v\hbar k_B^2 C_l}{\pi E_{\mathrm{def}}^2}\cdot\frac{1}{m_I^*}\cdot\left(\frac{{}^1F_{-2}^1}{{}^0F_{-2}^1}-\xi\right)^2 {}^0F_{-2}^1 \qquad (8)$$

$$zT = \frac{\left(\frac{{}^1F_{-2}^1}{{}^0F_{-2}^1}-\xi\right)^2}{\left[\frac{{}^2F_{-2}^1}{{}^0F_{-2}^1}-\left(\frac{{}^1F_{-2}^1}{{}^0F_{-2}^1}\right)^2\right]+\frac{1}{{}^{30}F_{-2}^1 B}}, \quad B = \frac{2Tk_B^2\hbar C_l N_v}{3\pi m_I^* E_{\mathrm{def}}^2 \kappa_L} \qquad (9)$$

Because the first term of eqn (8) only includes fundamental constants or composition independent material parameters in this study, the power factor (PF) is inversely proportional to m_I^* which is proportional to m^* in cubic materials. The third term of eqn (8) is a function of the reduced Fermi level and is optimized by doping. The thermoelectric figure of merit has a similar but slightly more complicated form (eqn (9)). Once the Fermi level is optimized by doping the maximum zT is determined by the *Quality Factor B*, first described by Chasmar and Stratton[9–12,61] for a parabolic band material. The quality factor is also inversely proportional to m_I^* (eqn (9)), providing direct relationship between high zT and low m_I^*.

The La- and I-doped materials at similar doping levels have similar total thermal conductivity (Fig. 2c). The higher electrical conductivity of I-doped materials leads to higher electronic contribution of thermal conductivity but this is compensated by a lower lattice thermal conductivity. This is partially explained by a ~3% reduced speed of sound (v_s) in I-doped samples (~1730 m s^{-1}) compared to that in La-doping samples (~1790 m s^{-1}). This leads to an expectation of ~10% lower lattice thermal conductivity in I-doping because the phonon scattering is dominated by the Umklapp process in single phased PbTe.[62] The higher sound velocity in La-doped materials should relate to the stiffer bonding between La and Te due to the low electronegativity of La. Microscope analysis on fracture surfaces shows no observable difference on the grain size between La- and I-doped PbTe, therefore, the lattice thermal conductivity difference cannot be explained by boundary scattering. It should be noted that the

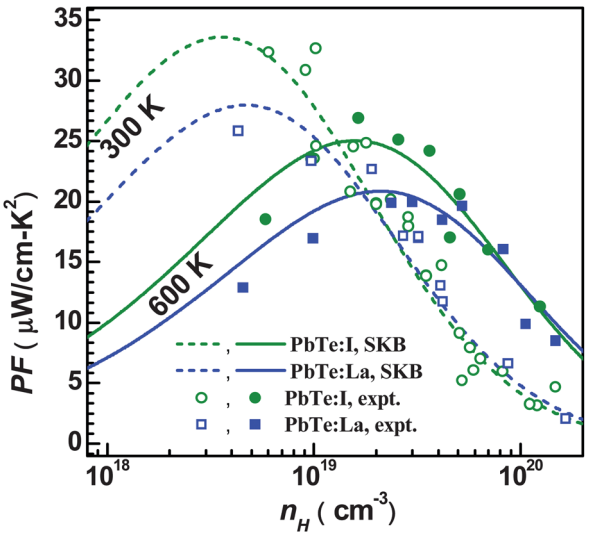

Fig. 5 Thermoelectric power factor *versus* Hall carrier concentration for La- and I-doped PbTe at the two end temperatures of 300 and 600 K. The 20% difference in effective mass due to variant dopant leads to the peak power factor differing by ~20% at both temperatures. The ~40% increase in effective mass (Fig. 3b), originating from the temperature increase from 300 to 600 K, results in a ~35% decrease in peak power factor in both La- and I-doped samples.

uncertainty on determining the lattice thermal conductivity can be as high as ~15% due to the combined errors from the thermal diffusivity (~5%) and resistivity (~5%) measurements.

With the known temperature dependent m^* for both La- and I-doped PbTe, use of the SKB model also enables an accurate prediction of the temperature dependent transport properties at any temperature and doping level. Fig. 2 also shows the calculated results (curves) having the same doping level as the actual samples, using the experimentally estimated lattice thermal conductivity.

Possessing a comparable thermal conductivity at similar doping levels (Fig. 2c) the La-doped series shows ~20% lower zT due to the ~20% higher m^* over the entire temperature range studied here, even though the Seebeck coefficient is higher, as compared to the I-doped samples. The observed higher zT in I-doping series can be explained by a combined effect of the higher power factor resulting from the lower effective mass and its lower lattice thermal conductivity.

There are subtle implications of this result to anisotropy that arises either from the crystal structure or the anisotropy of carrier pockets. It is beneficial to thermoelectric performance to have a lower inertial effective mass (m_I^*) for a given band effective mass (m_b^*). The ratio m_I^*/m_b^* depends on the anisotropy of carrier pockets and the direction of charge conduction. For anisotropic (not cubic) crystals the direction of lightest m_I^* is preferred for thermoelectric transport. In a cubic crystal differing m_I^*/m_b^* relies on the different averaging methods for $m_I^* = 3(1/m_1^* + 1/m_2^* + 1/m_3^*)^{-1}$ and $m_b^* = (m_1^* m_2^* m_3^*)^{1/3}$ for an anisotropic carrier pocket in three principle directions having effective masses of m_1^*, m_2^* and m_3^*.[26] However, an increased band effective mass (m_b^*) for a given, constant inertial effective mass (m_I^*) provides no obvious benefit, despite a higher Seebeck coefficient, when the scattering is dominated by nonpolar phonons.

It is known that dopants such as In,[63,64] Ti,[65–68] Cr[68–70] and Al[34] create resonant levels close to the conduction band edge in lead chalcogenides, which may affect the transport properties. However, there is no report showing that either I- or La-doping has a strong resonant level effect on PbTe. Unlike resonant doping systems that usually show a significant lower carrier concentration than the dopant concentration due to carrier localization,[65,71,72] each dopant atom (I or La) in this study produces one electron[28] in the conduction band according to the rules of valence.[40] The recently achieved high zT intrinsic to lead chalcogenides[27,28,32,34,61,73] was believed to be largely due to the different measurement of the thermal conductivity (κ) at high temperatures by the laser flash method (the most common technique today). Historical overestimation of κ led to a significant underestimation of zT in these materials.

In summary, we show an example of achieving higher thermoelectric performance as a result of lower effective mass, which is contrary to the generally held belief that higher effective mass is beneficial for thermoelectrics because of a higher Seebeck coefficient. It is demonstrated that the significant reduction of carrier mobility resulting from increased effective mass through band flattening actually reduces the thermoelectric power factor and zT in n-PbTe. Our efforts here have shown that the light band mass leads to higher performance and should be used as an important strategy for discovering and improving thermoelectric materials.

This work is supported by NASA-JPL and DARPA Nano Materials Program.

References

1 K. Biswas, J. He, Q. Zhang, G. Wang, C. Uher, V. P. Dravid and M. G. Kanatzidis, *Nat. Chem.*, 2011, **3**, 160–166.
2 P. F. P. Poudeu, J. D'Angelo, A. Downey, J. Short, T. Hogan and M. Kanatzidis, *Angew. Chem., Int. Ed.*, 2006, **45**, 3835–3839.
3 Y. Pei, J. Lensch-Falk, E. S. Toberer, D. L. Medlin and G. J. Snyder, *Adv. Funct. Mater.*, 2011, **21**, 241–249.
4 M. G. Kanatzidis, *Chem. Mater.*, 2010, **22**, 648–659.
5 M. Zebarjadi, K. Esfarjani, M. S. Dresselhaus, Z. F. Ren and G. Chen, *Energy Environ. Sci.*, 2012, **5**, 5147–5162.
6 Y. Pei, N. A. Heinz, A. LaLonde and G. J. Snyder, *Energy Environ. Sci.*, 2011, **4**, 3640–3645.
7 A. F. Ioffe, *Semiconductor Thermoelements, and Thermoelectric Cooling*, Infosearch, London, 1957.
8 G. J. Snyder and E. S. Toberer, *Nat. Mater.*, 2008, **7**, 105–114.
9 H. J. Goldsmid, *Thermoelectric Refrigeration*, Plenum Press, New York, 1964.
10 R. P. Chasmar and R. Stratton, *J. Electron. Control*, 1959, **7**, 52–72.
11 G. D. Mahan, in *Solid State Physics*, ed. H. Ehrenreich and F. Spaepen, Academic Press Inc, San Diego, 1998, vol. 51, pp. 81–157.
12 G. A. Slack, in *CRC Handbook of Thermoelectrics*, ed. D. M. Rowe, CRC Press, Boca Raton, Florida, 1995, ch. 34, pp. 406–440.
13 F. J. DiSalvo, *Science*, 1999, **285**, 703–706.
14 Y. Pei, X. Shi, A. LaLonde, H. Wang, L. Chen and G. J. Snyder, *Nature*, 2011, **473**, 66–69.
15 Y. Pei, A. D. LaLonde, N. A. Heinz, X. Shi, S. Iwanaga, H. Wang, L. Chen and G. J. Snyder, *Adv. Mater.*, 2011, **23**, 5674–5678.
16 O. Rabina, Y. Lin and M. Dresselhaus, *Appl. Phys. Lett.*, 2001, **79**, 81–83.
17 G. D. Mahan and J. O. Sofo, *Proc. Natl. Acad. Sci. U. S. A.*, 1996, **93**, 7436–7439.
18 J. P. Heremans, V. Jovovic, E. S. Toberer, A. Saramat, K. Kurosaki, A. Charoenphakdee, S. Yamanaka and G. J. Snyder, *Science*, 2008, **321**, 554–557.
19 J. A. Malen, S. K. Yee, A. Majumdar and R. A. Segalman, *Chem. Phys. Lett.*, 2010, **491**, 109–122.
20 T. E. Humphrey and H. Linke, *Phys. Rev. Lett.*, 2005, **94**, 096601.

21 J. Bardeen and W. Shockley, *Phys. Rev.*, 1950, **80**, 72–80.
22 C. Herring and E. Vogt, *Phys. Rev.*, 1956, **101**, 944–961.
23 J. M. Ziman, *Electrons and Phonons: The Theory of Transport Phenomena in Solids*, Clarendron, Oxford, 1960.
24 Y. I. Ravich, B. A. Efimova and I. A. Smirnov, *Semiconducting Lead Chalcogenides*, Plenum Press, New York, 1970.
25 R. W. Ure and R. R. Heikes, in *Thermoelectricity: Science and Engineering*, ed. R. R. Heikes and R. W. Ure, Interscience Publishers, New York, 1961, ch. 11, pp. 339–388.
26 Allowing for the ellipsoidal shape of the carrier pocket in cubic crystals with three principle directions having effective masses of m_1^*, m_2^* and m_3^*, one has $m_b^* = (m_1^* m_2^* m_3^*)^{1/3}$ and $m_I^* = 3(1/m_1^* + 1/m_2^* + 1/m_3^*)^{-1}$. Only when the carrier pocket is isotropic (even for cubic materials), with equal values of the three mass components of m_1^*, m_2^* and m_3^*, is m_I^* equal to m_b^*, although it is often a reasonable approximation.
27 Y. Pei, A. LaLonde, S. Iwanaga and G. J. Snyder, *Energy Environ. Sci.*, 2011, **4**, 2085–2089.
28 A. D. LaLonde, Y. Pei and G. J. Snyder, *Energy Environ. Sci.*, 2011, **4**, 2090–2096.
29 R. Blachnik and R. Igel, *Z. Naturforsch., B: Anorg. Chem., Org. Chem.*, 1974, **29**, 625–629.
30 O. Delaire, A. F. May, M. A. McGuire, W. D. Porter, M. S. Lucas, M. B. Stone, D. L. Abernathy, V. A. Ravi, S. A. Firdosy and G. J. Snyder, *Phys. Rev. B: Condens. Matter Mater. Phys.*, 2009, **80**, 184302.
31 M. Lach-hab, D. A. Papaconstantopoulos and M. J. Mehl, *J. Phys. Chem. Solids*, 2002, **63**, 833–841.
32 H. Wang, Y. Pei, A. D. LaLonde and G. J. Snyder, *Adv. Mater.*, 2011, **23**, 1366–1370.
33 Y. Pei, A. F. May and G. J. Snyder, *Adv. Energy Mater.*, 2011, **1**, 291–296.
34 Q. Zhang, H. Wang, W. Liu, H. Wang, B. Yu, Q. Zhang, Z. Tian, G. Ni, S. Lee, K. Esfarjani, G. Chen and Z. Ren, *Energy Environ. Sci.*, 2012, **5**, 5246–5251.
35 Y.-L. Pei and Y. Liu, *J. Alloys Compd.*, 2012, **514**, 40–44.
36 K. Biswas, J. He, G. Wang, S.-H. Lo, C. Uher, V. P. Dravid and M. G. Kanatzidis, *Energy Environ. Sci.*, 2011, **4**, 4675–4684.
37 K. Ahn, M. K. Han, J. Q. He, J. Androulakis, S. Ballikaya, C. Uher, V. P. Dravid and M. G. Kanatzidis, *J. Am. Chem. Soc.*, 2010, **132**, 5227–5235.
38 M. Zhou, J. F. Li and T. Kita, *J. Am. Chem. Soc.*, 2008, **130**, 4527–4532.
39 B. Volkov, L. Ryabova and D. Khokhlov, *Phys.-Usp.*, 2002, **45**, 819–846.
40 E. S. Toberer, A. F. May and G. J. Snyder, *Chem. Mater.*, 2010, **22**, 624–634.
41 Y. Pei, A. D. LaLonde, N. A. Heinz and G. J. Snyder, *Adv. Energy Mater.*, 2012, DOI: 10.1002/aenm.201100770.
42 Y. I. Ravich, B. A. Efimova and V. I. Tamarche, *Phys. Status Solidi B*, 1971, **43**, 11–33.
43 I. A. Smirnov and Y. I. Ravich, *Semiconductors*, 1967, **1**, 739–741.
44 M. K. Zhitinskaya, V. I. Kaidanov and I. A. Chernik, *Phys. Solid State*, 1966, **8**, 246.
45 Y. I. Ravich, B. A. Efimova and V. I. Tamarche, *Phys. Status Solidi B*, 1971, **43**, 453.
46 K. Ahn, C. P. Li, C. Uher and M. G. Kanatzidis, *Chem. Mater.*, 2009, **21**, 1361–1367.
47 G. T. Alekseeva, M. V. Vedernikov, E. A. Gurieva, P. P. Konstantinov, L. V. Prokof'eva and Y. I. Ravich, *Semiconductors*, 1998, **32**, 716–719.
48 T. S. Stavitskaya, V. A. Long and B. A. Efimova, *Phys. Solid State*, 1966, **7**, 2062.
49 G. T. Alekseeva, E. A. Gurieva, P. P. Konstantinov, L. V. Prokofeva and M. I. Fedorov, *Semiconductors*, 1996, **30**, 1125–1127.
50 B. A. Efimova, L. A. Kolomoets, Y. I. Ravich and T. S. Stavitskaya, *Semiconductors*, 1971, **4**, 1653–1658.
51 Y. Gelbstein, Z. Dashevsky and M. P. Dariel, *Phys. B*, 2005, **363**, 196–205.
52 R. W. Fritts, in *Thermoelectric Materials and Devices*, ed. I. B. Cadoff and E. Miller, Reinhold Pub. Corp., New York, 1960, pp. 143–162.
53 H. A. Lyden, *Phys. Rev. [Sect.] A*, 1964, **135**, A514–A521.
54 R. N. Tauber, A. A. Machonis and I. B. Cadoff, *J. Appl. Phys.*, 1966, **37**, 4855–4860.
55 A. Gibson, *Proc. Phys. Soc., London, Sect. B*, 1952, **65**, 378–388.
56 Y. I. Ravich, in *Lead Chalcogenides: Physics and Applications*, ed. D. Khokhlov, Taylor & Fransics Group, New York, 2003, pp. 1–34.
57 E. Kane, *J. Phys. Chem. Solids*, 1957, **1**, 249–261.
58 I. A. Smirnov, B. Y. Moizhes and E. D. Nensberg, *Phys. Solid State*, 1961, **2**, 1793–1804.
59 T. S. Stavitskaya, I. V. Prokofev, Y. I. Ravich and B. A. Efimova, *Semiconductors*, 1968, **1**, 952–956.
60 L. Rogers, *J. Phys. D: Appl. Phys.*, 1971, **4**, 1025.
61 A. D. LaLonde, Y. Pei, H. Wang and G. J. Snyder, *Mater. Today*, 2011, **14**, 526–532.
62 E. Toberer, A. Zevalkink and G. J. Snyder, *J. Mater. Chem.*, 2011, **21**, 15843–15852.
63 V. I. Kaidanov, S. A. Nemov and Y. I. Ravich, *Semiconductors*, 1992, **26**, 113–125.
64 A. A. Averkin, V. I. Kaidanov and R. B. Melnik, *Semiconductors*, 1971, **5**, 75.
65 M. N. Vinogradova, E. A. Gurieva, V. I. Zharskii, S. V. Zarubo and L. V. Prokofeva, *Semiconductors*, 1978, **12**, 387–390.
66 F. Sizov, V. Teterkin, L. Prokofeva and E. Gurieva, *Semiconductors*, 1980, **14**, 1063–1064.
67 J. Koenig, M. Nielsen, Y.-B. Gao, M. Winkler and A. Jacquot, *Phys. Rev. B: Condens. Matter Mater. Phys.*, 2011, **84**, 205126.
68 V. V. Teterkin, F. F. Sizov, L. V. Prokofeva, Y. S. Gromovoi and M. N. Vinogradova, *Semiconductors*, 1983, **17**, 489–491.
69 M. D. Nielsen, E. M. Levin, C. M. Jaworski, K. Schmidt-Rohr and J. P. Heremans, *Phys. Rev. B: Condens. Matter Mater. Phys.*, 2012, **85**, 045210.
70 M. I. Baleva and L. D. Borissova, *J. Phys. C: Solid State Phys.*, 1983, **16**, L907–L911.
71 V. I. Kaidanov and Y. I. Ravich, *Usp. Fiz. Nauk*, 1985, **145**, 51–86.
72 J. P. Heremans, B. Wiendlocha and A. M. Chamoire, *Energy Environ. Sci.*, 2012, **5**, 5510–5530.
73 S. Wang, G. Zheng, T. Luo, X. She and H. Li, *J. Phys. D: Appl. Phys.*, 2011, **44**, 475304.